A new cobalt(II) complex nanosheet as an electroactive medium for plasmonic switching on Au nanoparticles

Yurong Liu[a,c] Wenzheng Lu,[d] Xizhe Cheng,[d] Jianfang Wang,[d*] and Wai-Yeung Wong[a,b,c*]

2D metal-organic complex nanosheets with the merits of high stability and structure tunability are an emerging topic in recent years. To extend the promising ultrathin architectures, a new Co(II) complex nanosheet (**Co-nanosheet**) is designed and prepared via a readily operated interface-assisted coordination reaction between the ligand 4,4'',4'''-(2,4,6-trimethylbenzene-1,3,5-triyl)tris(2,2':6',2"-terpyridyl) (**L**) and Co2+ ion. The formed Co(II) complex nanosheet exhibits both uniform layered structure and good thermostability as proposed, which was verified by various chemical and physical analytical methods. Moreover, it is firstly utilized as an electroresponsive medium to tune the surface plasmon resonance behavior of Au nanoparticles, expanding the applicable fields of this type of 2D materials.

Keywords: metal-organic complex nanosheet, layered structures, electroactive medium, plasmonic switching

Introduction

Bottom-up nanosheets are a class of attractive 2D materials which are directly generated from the assembly of small molecules or ions rather than the exfoliation of bulk mother crystals, and thus feature high flexibility in building blocks as compared with the opposite top-down nanosheets.[1–4] Among them, the metal-organic complex nanosheets, with bonds formed via coordination reaction of ligands and metal ions, could efficiently expand the diversity of these 2D frameworks considering the various combination of the organic ligands and inorganic metal ion components.[5–7] More importantly, the metal-organic nanosheets play an increasing important role in diverse application fields.[8,9] Terpyridine as a planar tridentate ligand plays an important role in transition metal complexes.[10,11] It could chelate Co(II) in a spontaneous and rational manner to form tpy-Co(II) motif, displaying suitable chelating reversibility and bond robustness.

On the other hand, it has been found that noble metal nanoparticles (NPs) such as gold (Au), silver (Ag), platinum (Pt) could exhibit localized surface plasmon resonance (LSPR) effect.[12] Active plasmonics is a burgeoning subfield of plasmonics. The LSPR-adjustable plasma device (such as plasma switch, modulator, *etc*.) is a kind of important micro-optoelectronic components, which gives great application prospects in information reading and writing, storage and processing, as well as wearable devices, smart home and other fields.[13–16] However, it is difficult to realize the LSPR switching by directly applied external physical stimuli towards the bare plasmonic metal NPs (*e.g.* Au NPs), and consequently the additional stimuli-responsive medium is necessary for the construction of active plasmonic composite systems.[17] Recent reported active media mainly include graphene,[18,19] liquid crystals[20] and conductive polymers.[21] Yet they often suffer from the limited structural diversity and

flexibility. By contrast, metal-organic nanosheets which feature tailored structures and properties by taking advantages of both metal ions and ligands, may endow the materials with diverse stimuli-responsive performance (such as electric or magnetic responsiveness).[22,23] Then, the coupling of excitons in 2D nanosheet medium and the plasmons in Au NPs may be modulated. In this context, it is likely to achieve the desired fine-tuning of LSPR under a low stimulus signal input by constructing nanosheets-Au NPs composites, where the excitons in these nanosheets can be designed to be controllable by electric or magnetic fields through the proper selection of metal ions and organic ligands. Moreover, the combined structure-controllable 2D nanosheet and 0D Au NPs with LSPR may exhibit synergistic effect within the formed novel active plasmonic composite materials as potential building blocks for quantum information systems, ultralow threshold single-photon sources and lasers.[24,25]

Herein, a new nanosheet (**Co-nanosheet**) based on arene-centred three-way terpyridine ligand 4,4'',4'''-(2,4,6-trimethylbenzene-1,3,5-triyl)tris(2,2':6',2"-terpyridyl) (**L**) is synthesized. Considering the reported electrochemical activity of these materials,[26] **Co-nano sheet** is applied as an electroactive medium to achieve LSPR switching on gold NPs, which expand the functionality of this kind of metal complex nanosheets. We deposit the pre-synthesized Au NPs onto the nanosheet to form composites and investigate the LSPR tuning behavior by measuring the ensemble extinction spectra and single-particle dark-field scattering spectra. The study is expected to enrich plasmon modes and therefore allow more flexibility in LSPR control. Also, the major emphasis of this primary work presented here is to prove the switching concept of the combination of switchable 2D materials and Au NPs, especially in the presence of the coupling between the nanosheets and Au NPs, where they both have a flat surface.

Results and discussion

The structure of the ligand **L** is displayed in Figure 1. The nanosheet **Co-nanosheet** is prepared through coordination of **L** and Co^{2+} ion while the Cl^- from $CoCl_2{\cdot}6H_2O$ works as a counter anion to make the product charge neutral. The metal-organic coordination bond theoretically can be spontaneously and rationally formed, making a good balance of reversibility and robustness, and leading to less structural defects. So, the ideal topological structure of the formed sheet is shown in Figure 1 and the counter anions are omitted for clarity. Note that the coordination geometry of the Co(II) ions is octahedral. Therefore, the formed nanosheet is different from the well-defined 2D graphene and is not completely planar in molecular level, which will be rippled, and has a significant third dimension for each layer. However, the layers of the nanosheet are noncovalently connected.[23]

According to the pioneering work[17,26–28] on the interface-assisted synthetic method, multilayer **Co-nanosheet** with several hundred nanometer thick is prepared in a cylindrical vial. As shown in Figure 2a, a transparent pale-yellow film is visible at the liquid-liquid interface. It is worth noting that if the initially formed thin film is broken by the air bubbles caused by the vaporization of the dichloromethane (DCM) during reaction, the nanosheet could recover to be intact at the interface as displayed in Figure S5, which might suggest the

repairability and epitaxial capability of the nanosheets. Besides, **Co-nanosheet** is insoluble in both organic solvents and aqueous solution, supporting the polymeric structure as proposed. It is also stable both in air and in solution. According to the TGA result (Figure S6), less than 20% weight is lost after raising the system temperature up to 500 °C. Therefore, it exhibits satisfactory thermal stability, reflecting the robustness of the coordination bonds between tpy and Co^{2+}.

Co-nanosheet is then characterized after being transferred onto Si, quartz substrates and copper grids, respectively. Several types of microscopes including optical microscope (OM), field-emission scanning electron microscope (FE-SEM), transition electron microscope (TEM) and atomic force microscope (AFM) are used to gain the morphological information. According to the OM image (Figure 2b), **Co-nanosheet** shows a flat and monolithic sheet morphology with domain size in one side up to about 1 cm. The SEM and TEM images are displayed in Figure 2c and 2d, respectively. The multilayer **Co-nanosheet** deposited on a Si substrate is easily distinguished from the bare substrate in the SEM image and the smooth surface and uniform texture as a sheet is further evidenced. The obtained TEM result indicates the layered structure of **Co-nanosheet** as expected. The uniform sheet shows a lighter contrast relative to the bare silicon in the AFM height image while in the phase image, the nanosheet is evenly spread out on the Si substrate (Figure 2e). The cross-sectional analysis discloses the thickness of the multilayer nanosheet to be ~330 nm. The energy dispersive X-ray spectrometer coupled with SEM (SEM/EDX), X-ray photoelectron spectrometer (XPS) and Fourier transform infrared spectrometer (FT-IR) were applied for structural analysis of the synthesized nanosheet. The SEM/EDX mapping images for C, N, Co, Cl, and Si are shown in Figure 2f, demonstrating the homogeneity of the formed nanosheet.

The wide scan XP spectra of **L** (Figure S7a) and **Co-nanosheet** (Figure S8b) reveal that the elements C, N within **Co-nanosheet** should come from the ligand part while the Co and Cl are from the metal salt as proposed (O should be from atmosphere and Si is from the substrate), confirming the complexation between the ligand and Co^{2+}. Here, a complex $[Co(tpy)_2](BF_4)_2 \cdot H_2O$ (**R**) (structure is shown in Figure S7c) is synthesized and characterized as a reference molecule. The full XP spectrum of **R** (Figure S7d) shows a similar result with that of **Co-nanosheet**. As for the narrow scan spectra (see Figure 2g), the N 1s peak of **L** is shifted up from 398.21 eV to 399.93 eV upon the formation of **Co-nanosheet** which is close to that of **R** (399.69 eV), thus providing further evidence of the coordination between **L** and Co^{2+}. The binding energies of Co 2p core level of **Co-nanosheet** and **R** are similar too, also ensuring the completed complexation. The peak of **R** at 193.39 eV should be attributed to B 1s core level which is different from the Cl 2p core level of **Co-nanosheet**. The FT-IR spectra of them are then compared in Figure S8. The C = C stretching vibration peak of **L** is visible at 1585 cm^{-1} while that of the corresponding nanosheet **Co-nanosheet** shifts to a higher wavenumber at 1610 cm^{-1}, which is much close to that of **R** (1600 cm^{-1}). The peak variation is a typical phenomenon for terpyridine ligands on complexation to metal ions. Moreover, the intensity of the sharp weak peak of C = N stretching vibration of **L** at 1648 cm^{-1} becomes weaker when the corresponding nanosheet **Co-nanosheet** is formed, which may be due to the weakened C = N double bond caused by the formation of metal-N bond after complexation. Neither X-ray

nor electron diffraction was observed for **Co-nanosheet**, presumably due to the disordered location of the counteranion (Cl^-) or the chaotic stacking of the layers.[26]

After **Co-nanosheet** is well characterized, the preliminary study on the electrochemical switching of the plasmons of Au nanoplates has been carried out. At first, the hexagonal shaped gold nanoparticles (Au NPs) with the lateral size of 150 ± 4 nm and thickness of 40 ± 2 nm were prepared (Figure 3a). The extinction spectrum of the formed Au NPs in water solution was also obtained as shown in Figure 3b with a maximum extinction intensity at 725 nm. Then, the nanosheet was deposited on transparent conductive substrates, such as indium tin oxide (ITO)-coated glass slides followed by dropping of the Au NPs onto the nanosheet to form a composite (Au@**Co-nanosheet**) (Figure S9). Here, the plasmonic switching of Au@**Co-nanosheet** was observed in single-particle level by the combined techniques as described in the reported work[29]. The ITO glass, with Au NPs physically adsorbed **Co-nanosheet** was used as the working electrode, Ag/AgCl worked as the reference electrode and Pt wire was applied as the counter electrode in a three-electrode system with tetrabutyl ammonium hexafluorophosphate ($TBAPF_6^-$) /acetonitrile as the electrolyte. The CV curves in the negative and positive window were respectively acquired with a scan rate of 0.05 V/s (Figure 4a and 4b). The positive scan of as-prepared Au@**Co-nanosheet** resulted in a stable quasi-reversible redox wave at around 0.35 V, which should be assigned to the redox couple of Co^{2+}/Co^{3+}. When it was negatively scanned to -1.6 V, there was a pair of redox peaks at around -0.6 V belonging to Co^{2+}/Co^{+}. As these species in solution could freely diffuse, the contribution caused by electron self-exchange is negligible. However, when they are confined at electrodes where physical diffusion is slower by many orders of magnitude, the effect of self-exchange on faradaic current density could be remarkable, and even dominant. The different self-exchange rate for Co^{2+}/Co^{3+} (k = 2 M^{-1} s^{-1})[30] and Co^{2+}/Co^{+} (k = 10^8 M^{-1} s^{-1})[31] results in a noticeable distinction in their current density (order of magnitude is 10 μA and 10^3 μA, respectively), which is in good agreement with their electrochemical behavior in a surface-restrained environment. Another peak at around -1.5 V may be caused by the displacement of the tpy ligand with the moderately strong monodentate acetonitrile to form two bis(coordinated) tpy or a tris(coordinated) tpy and monocoordinated tpy. Therefore, the small peak at around -1.3 V may be contributed by the couple of $[Co(tpy)_2(acetonitrile)_2]^+/[Co(tpy)_2(acetonitrile)_2]^{2+}$, according to the previous study.[32]

Next, three voltages are selected in the switching test, that is +0.8 V, +0.1 V and -1.0 V. The recorded switching current-time curves (i–t curves) are shown in Figure S10. The applied voltage of 0.8 V leads to an oxidation current of 1.2 μA while the latter applied voltage of 0.1 V results in a reduction current of -3.0 μA. The difference in current density conforms to the CV results. Besides, the current decays with time, indicating the consumption of reagent as aforementioned, while a current peak was observed when -1.0 V was applied, implying some other electron transport processes. The scattering spectra of Au@**Co-nanosheet** under different applied voltages are recorded as shown in Figure 4c. The plasmon peaks of both in-plane dipole mode (around 700 nm) and in-plane quadrupole mode (around 600 nm) are blue-shifted with voltage varying from +0.1 V to -1.0 V, but no obvious change is observed from +0.8 V to +0.1 V. The plasmon peak of in-plane dipole mode shows a noteworthy plasmonic shift of ~ 25 nm, reflecting the diminished refractive index of **Co-nanosheet** during the

electrochemical process. Overall, active plasmon switching is observed by changing the applied potentials towards the nanosheet-Au NPs system. Although the switching performances, including the modulation depth and the peak shift need to be improved, this type of metal complex nanosheet still has the potential to realize the switchable plasmonic behavior of Au NPs through further rational structure design and property modulation.

Experimental

Synthetic procedures

General procedure for the synthesis of Co-nanosheet: 5.0×10^{-5} mol L^{-1} DCM solution of **L** (lower layer: 10 mL) and 5.0×10^{-2} mol L^{-1} aqueous solution containing excessive Co^{2+} ion (upper layer: 20 mL) were used to create a liquid-liquid interface in a clean and oven-dried cylindrical vial with the volume of 50 mL and diameter of 3.2 cm. A small piece of pretreated substrate (such as 1 cm × 1 cm silicon and quartz) was placed at the bottom. The whole system was kept undisturbed for 3 weeks under ambient conditions to form a transparent pale-yellow film at the liquid-liquid interface.

General procedure for the synthesis of $[Co(tpy)_2](BF_4)_2 \cdot H_2O$ (R): The $Co(BF_4)_2 \cdot 6H_2O$ (62.2 mg, 168.6 μmol) was dissolved into 10 mL water to prepare an aqueous solution. Then, 2,2´:6´,2´´-terpyridine (85.2 mg, 366 μmol) was added. The reaction system was vigorously stirred for 5 h. After that, the precipitant was filtered out and excess ammonium tetrafluoroborate water solution (1 g in 10 mL water) was poured into the filtrate. The obtained orange precipitant was filtered, washed by a small amount of water, iced methanol and then oven-dried (15 mg, yield 12.4%). Elemental analysis was conducted, found, N 11.69, C 50.54, H 3.23; calculated for $C_{30}H_{22}N_6B_2F_8Co \bullet H_2O$, N 11.72, C 50.25, H 3.62.

Transfer of the nanosheets onto substrates and TEM grids

For TEM test, small pieces were transferred to the copper grids by pipetting the suspension containing **Co-nanosheet** and then dried under a nitrogen blow. Besides, **Co-nanosheet** can be deposited onto the previously placed substrate on the vial bottom by carefully removing the upper water solution and lower organic solvent in sequence by syringes. It also could be directly transferred to substrates with tweezers, and the modified substrates were dried *in vacuo* overnight before the measurements.

Electrochemical measurements

The CH Instruments Model 600 D Serials Potentials was employed to conduct electrochemical research work with a three-electrode set-up (working electrode: ITO glasses modified with **Co-nanosheet**, reference electrode: Ag/AgCl, counter electrode: Pt wire). All electrolytes were degassed with dry argon and all measurements were performed under an argon atmosphere. The dark-field scattering spectra in single-particle level were obtained by an Olympus BX60 optical microscopy equipped with a tungsten-halogen lamp, a monochromator and a charge coupled device camera. The single-particle electrochemical plasmonic performance data were recorded by combining the scattering spectrometry and electrochemical working station, as shown in Scheme S1.

Conclusions

An arene-centred three-way terpyridine ligand **L** is synthesized to generate the corresponding multilayer Co(II) complex nanosheet **Co-nanosheet** via a mild interface-assisted process. The structure of the formed nanosheet is well characterized by various microscopies, SEM/EDX mapping, XPS and FTIR techniques. Besides, the pale-yellow **Co-nanosheet** shows the merits of good mechanism strength and optical transparency, which is desired in flexible electronic devices. Finally, **Co-nanosheet** is used as the active media together with Au NPs to construct 2D-0D composite system, aiming at realizing electrochemical potential-controlled active plasmon switching by getting the utmost of the structurally adjustable characteristics of the nanosheet and the LSPR effect of Au NPs. More systematic studies are on-going to understand the switching mechanisms and promote the switching performances in terms of the changes in the modulation depth and peak shift, and the presented primary work clearly provides a proof of concept demonstration for further study.

Conflicts of interest

There are no conflicts to declare.

Acknowledgements

W.-Y. Wong thanks the Science, Technology and Innovation Committee of Shenzhen Municipality (JCYJ20180507183413211), the National Natural Science Foundation of China (No. 52073242), the RGC Senior Research Fellowship Scheme (SRFS2021-5S01), the Hong Kong Research Grants Council (PolyU 153058/19P), the Hong Kong Polytechnic University (1-ZE1C) and the Endowed Professorship in Energy from Ms Clarea Au (847S) for the financial support. Y. Liu would like to thank the China Postdoctoral Science Foundation Funded Project (2020M672817).

Notes and references

1 C. E. Boott, A. Nazemi and I. Manners, *Angew. Chem. Int. Ed.*, 2015, **54**, 13876–13894.

2 P. Payamyar, B. T. King, H. C. Öttinger and A. D. Schlüter, *Chem. Commun.*, 2016, **52**, 18–34.

3 D. Rodríguez-San-Miguel, P. Amo-Ochoa and F. Zamora, *Chem. Commun.*, 2016, **52**, 4113–4127.

4 Y. Liu, W. Deng, Z. Meng and W.-Y. Wong, *Small*, 2020, **16**, 1905204.

5 T. Kambe, T. Kusamoto, R. Sakamoto and H. Nishihara, *Macromol. Symp.*, 2015, **351**, 78–80.

6 A. J. Clough, J. W. Yoo, M. H. Mecklenburg and S. C. Marinescu, *J. Am. Chem. Soc.*, 2015, **137**, 118–121.

7 T. Bauer, Z. Zheng, A. Renn, R. Enning, A. Stemmer, J. Sakamoto and A. D. Schlüter, *Angew. Chem. Int. Ed.*, 2011, **50**, 7879–7884.

8 G. Lan, Z. Li, S. S. Veroneau, Y.-Y. Zhu, Z. Xu, C. Wang and W. Lin, *J. Am. Chem. Soc.*, 2018, **140**, 12369–12373.
9 J.-W. Wang, L.-Z. Qiao, H.-D. Nie, H.-H. Huang, Y. Li, S. Yao, M. Liu, Z.-M. Zhang, Z.-H. Kang and T.-B. Lu, *Nat. Commun.*, 2021, **12**, 813.
10 X. Lu, X. Li, K. Guo, T.-Z. Xie, C. N. Moorefield, C. Wesdemiotis and G. R. Newkome, *J. Am. Chem. Soc.*, 2014, **136**, 18149–18155.
11 C.-Y. Hsu, J. Zhang, T. Sato, S. Moriyama and M. Higuchi, *ACS Appl. Mater. Interfaces*, 2015, **7**, 18266–18272.
12 H. A. Atwater and A. Polman, *Nat. Mater.*, 2010, **9**, 205–213.
13 D. K. Gramotnev and S. I. Bozhevolnyi, *Nat. Photonics*, 2010, **4**, 83–91.
14 J. A. Schuller, E. S. Barnard, W. Cai, Y. C. Jun, J. S. White and M. L. Brongersma, *Nat. Mater.*, 2010, **9**, 193–204.
15 K. M. Mayer and J. H. Hafner, *Chem. Rev.*, 2011, **111**, 3828–3857.
16 S. Linic, U. Aslam, C. Boerigter and M. Morabito, *Nat. Mater.*, 2015, **14**, 567–576.
17 Y. Liu, R. Sakamoto, C.-L. Ho, H. Nishihara and W.-Y. Wong, *J. Mater. Chem. C*, 2019, **7**, 9159–9166.
18 Y. Yao, M. A. Kats, P. Genevet, N. Yu, Y. Song, J. Kong and F. Capasso, *Nano Lett.*, 2013, **13**, 1257–1264.
19 J. Kim, H. Son, D. J. Cho, B. Geng, W. Regan, S. Shi, K. Kim, A. Zettl, Y.-R. Shen and F. Wang, *Nano Lett.*, 2012, **12**, 5598–5602.
20 S. Khatua, W.-S. Chang, P. Swanglap, J. Olson and S. Link, *Nano Lett.*, 2011, **11**, 3797–3802.
21 Y. Leroux, E. Eang, C. Fave, G. Trippe and J. C. Lacroix, *Electrochem. Commun.*, 2007, **9**, 1258–1262.
22 R. Dong, M. Pfeffermann, H. Liang, Z. Zheng, X. Zhu, J. Zhang and X. Feng, *Angew. Chem. Int. Ed.*, 2015, **54**, 12058–12063.
23 R. Sakamoto, K. Hoshiko, Q. Liu, T. Yagi, T. Nagayama, S. Kusaka, M. Tsuchiya, Y. Kitagawa, W.-Y. Wong and H. Nishihara, *Nat. Commun.*, 2015, **6**, 6713.
24 T. Xu, E. C. Walter, A. Agrawal, C. Bohn, J. Velmurugan, W. Zhu, H. J. Lezec and A. A. Talin, *Nat. Commun.*, 2016, **7**, 10479.
25 G. Garcia, R. Buonsanti, E. L. Runnerstrom, R. J. Mendelsberg, A. Llordes, A. Anders, T. J. Richardson and D. J. Milliron, *Nano Lett.*, 2011, **11**, 4415–4420.
26 K. Takada, R. Sakamoto, S.-T. Yi, S. Katagiri, T. Kambe and H. Nishihara, *J. Am. Chem. Soc.*, 2015, **137**, 4681–4689.
27 T. Kambe, R. Sakamoto, K. Hoshiko, K. Takada, M. Miyachi, J.-H. Ryu, S. Sasaki, J. Kim, K. Nakazato, M. Takata and H. Nishihara, *J. Am. Chem. Soc.*, 2013, **135**, 2462–2465.
28 T. Tsukamoto, K. Takada, R. Sakamoto, R. Matsuoka, R. Toyoda, H. Maeda, T. Yagi, M. Nishikawa, N. Shinjo, S. Amano, T. Iokawa, N. Ishibashi, T. Oi, K. Kanayama, R. Kinugawa, Y. Koda, T. Komura, S. Nakajima, R. Fukuyama, N. Fuse, M. Mizui, M.

Miyasaki, Y. Yamashita, K. Yamada, W. Zhang, R. Han, W. Liu, T. Tsubomura and H. Nishihara, *J. Am. Chem. Soc.*, 2017, **139**, 5359–5366.

29 W. Lu, N. Jiang and J. Wang, *Adv. Mater.*, 2017, **29**, 1604862.

30 B. R. Baker, F. Basolo and H. M. Neumann, *J. Phys. Chem.*, 1959, **63**, 371–378.

31 B. S. Brunschwig, C. Creutz, D. H. Macartney, T.-K. Sham and N. Sutin, *Faraday Discuss. Chem. Soc.*, 1982, **74**, 113.

32 A. R. Guadalupe, D. A. Usifer, K. T. Potts, H. C. Hurrell, A. E. Mogstad and H. D. Abruna, *J. Am. Chem. Soc.*, 1988, **110**, 3462–3466.

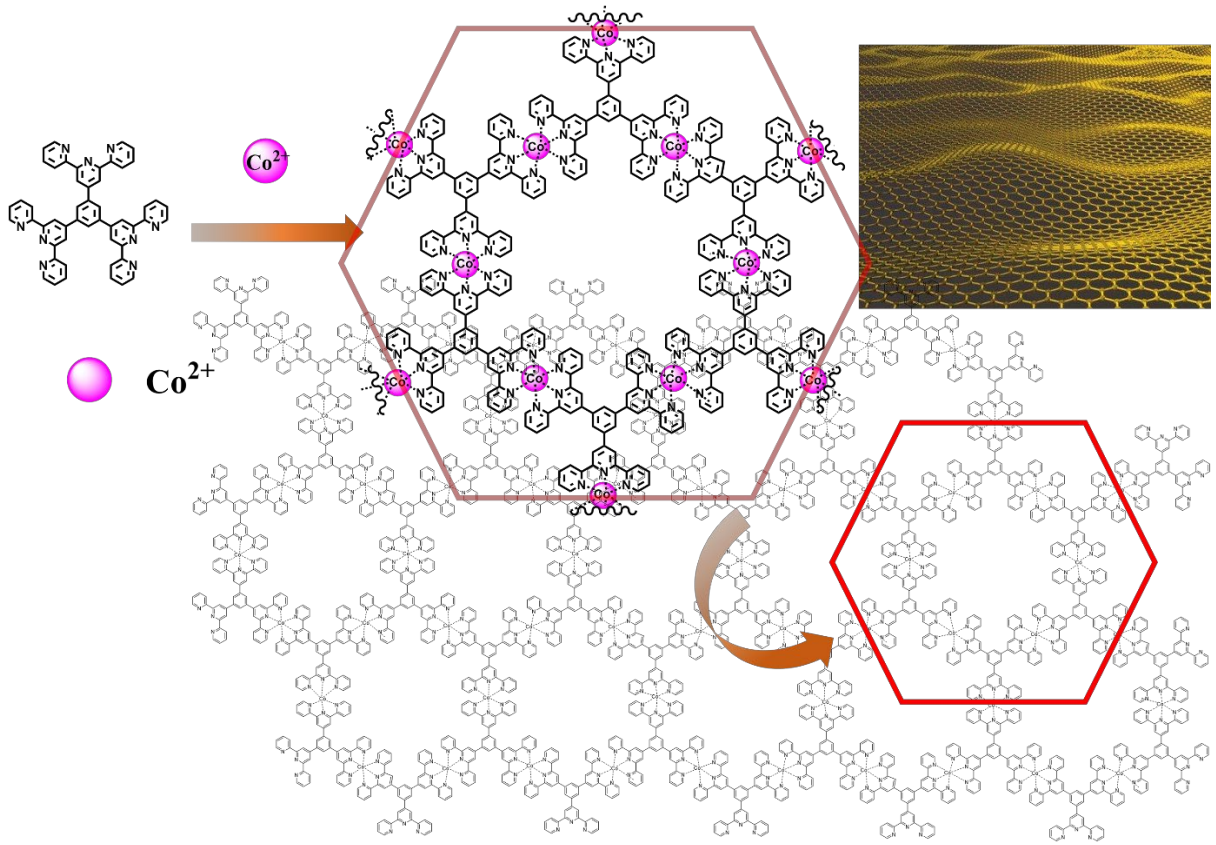

Figure 1. The schematic diagram of the formation of the nanosheet **Co-nanosheet** from the ligand **L**.

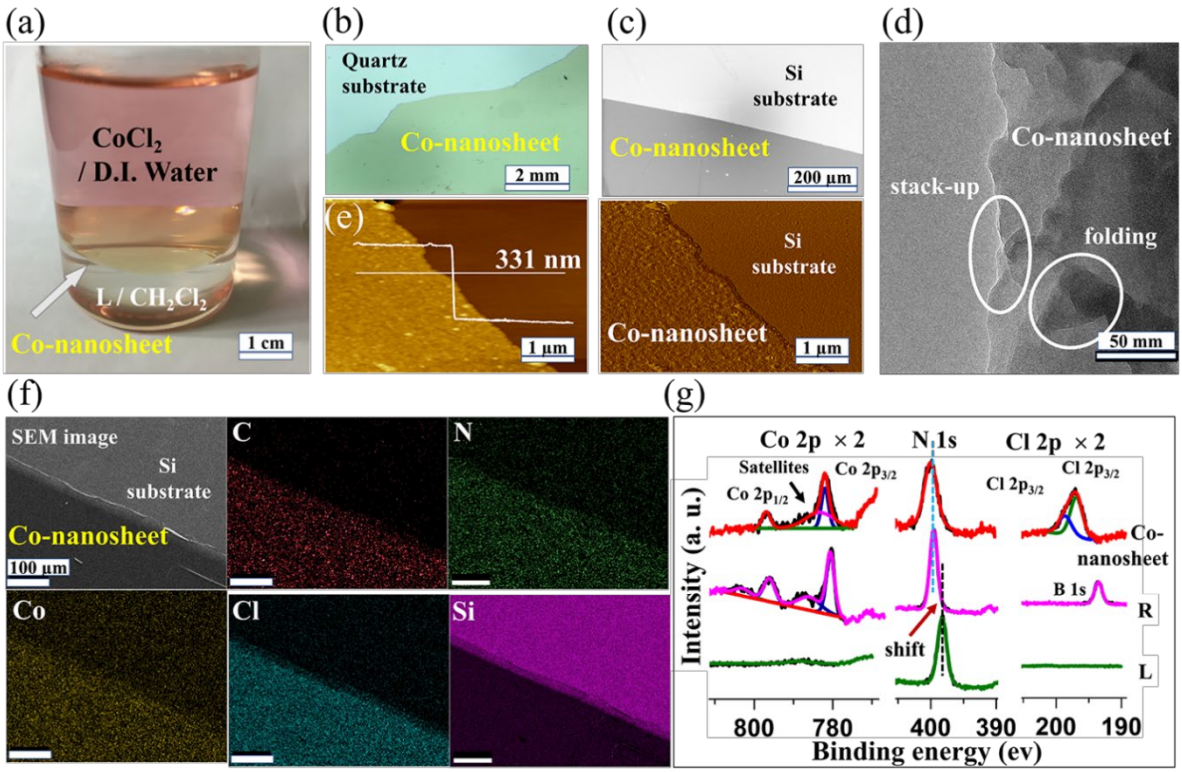

Figure 2. Synthesis and characterization of **Co-nanosheet**. a) The photograph of **Co-nanosheet** at the interface in the reaction container. b) The OM image of **Co-nanosheet** on quartz substrate. c) The SEM images of **Co-nanosheet** on Si substrate. d) The TEM image of **Co-nanosheet** on copper grid. e) The AFM images and cross-sectional analysis of **Co-nanosheet** on Si substrate: the left one is height image and the right one is phase image. Cross-sectional analysis was performed along with the white line in height image. f) The SEM/EDX mapping images of **Co-nanosheet** for elements C, N, Co, Cl, Si. g) The comparison of narrow XP spectra among **Co-nanosheet**, **R** and **L** focusing on N 1s, Co 2p, and Cl 2p core levels, respectively.

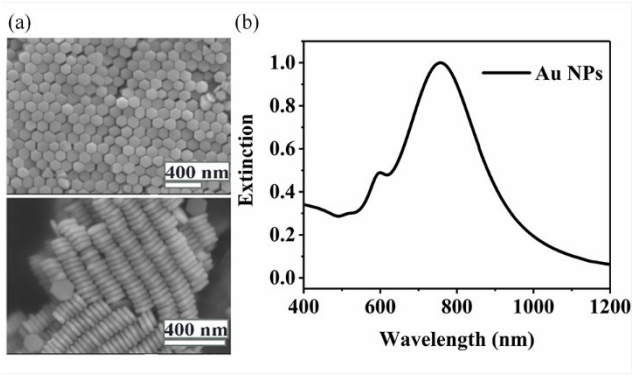

Figure 3. a) The morphology of the used Au NPs with the lateral size of 150 ± 4 nm and thickness of 40 ± 2 nm. b) The extinction spectrum of Au NPs.

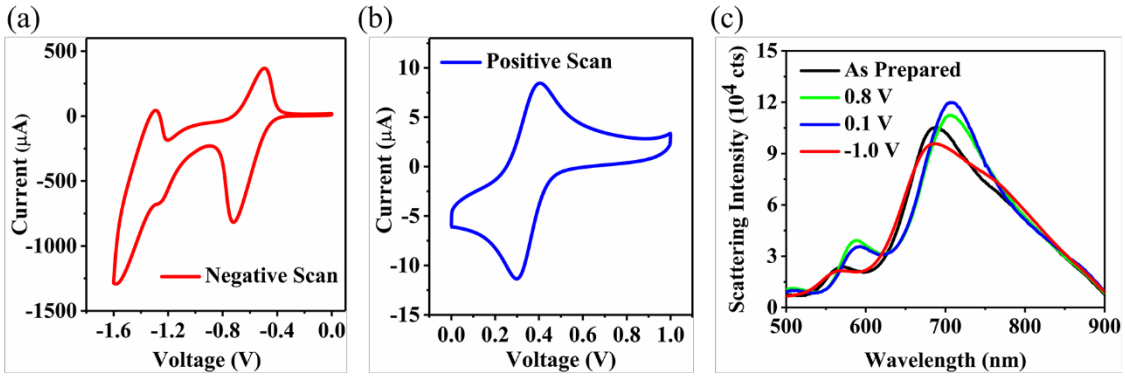

Figure 4. Cyclic voltammetry curves of Au@**Co-nanosheet** a) in a negative window and b) in a positive window at a scan speed of 0.05 V/s. c) Dark-field scattering spectra of Au@**Co-nanosheet**.